

Engineering drag currents in Coulomb coupled quantum dots

Jong Soo Lim¹, David Sánchez² and Rosa López²

¹School of Physics, Korea Institute for Advanced Study, Seoul 130-722, Korea

²Institute for Cross-Disciplinary Physics and Complex Systems IFISC (UIB-CSIC), E-07122 Palma de Mallorca, Spain

E-mail: david.sanchez@uib.es

Abstract. The Coulomb drag phenomenon in a Coulomb-coupled double quantum dot system is revisited with a simple model that highlights the importance of simultaneous tunneling of electrons. Previously, cotunneling effects on the drag current in mesoscopic setups have been reported both theoretically and experimentally. However, in both cases the sequential tunneling contribution to the drag current was always present unless the drag level position were too far away from resonance. Here, we consider the case of very large Coulomb interaction between the dots, whereby the drag current needs to be assisted by cotunneling events. As a consequence, a quantum coherent drag effect takes place. Further, we demonstrate that by properly engineering the tunneling probabilities using band tailoring it is possible to control the sign of the drag and drive currents, allowing them to flow in parallel or antiparallel directions. We also show that the drag current can be manipulated by varying the drag gate potential and is thus governed by electron- or hole-like transport.

1. Introduction

In a system made of two nearby (electrically) isolated conductors where particles are prevented from tunneling into each other, a bias drop through one conductor can drag a current through the other conductor due to Coulomb interaction between them [1, 2]. The Coulomb drag effect was first suggested by Pogrebinskii [3] and Price [4] theoretically and explained by energy and momentum transfer from the drive conductor to the drag conductor due to Coulomb mutual friction. This phenomenon has become a quite useful toolbox to probe electron-electron or electron-hole scattering mechanisms in many-body systems. At the early stage, the effect has been observed in semiconductor 2D-3D electron gas layers [5], 2D-2D electron gas layers [6], 2D electron gas-2D hole gas layers [7] and then investigated under the influence of a perpendicular magnetic field [8, 9, 10, 11, 12, 13, 14, 15, 16, 17]. Since the Coulomb interaction is stronger in 1D than 2D, Coulomb drag between 1D-1D quantum nanowires has been also extensively explored [18, 19, 20, 21]. More recently, interest has shifted to more exotic systems such as graphene double layers [22, 23, 24], graphene double ribbons [25], graphene-2D electron gases [26], or double bilayer graphene heterostructures [27]. In addition, Coulomb drag between electrostatically coupled arrays of metallic tunnel junctions [28, 29], between quantum wire and quantum dot [30], between quantum dots [31], or between quantum point contacts [32] has been demonstrated. In such systems translational symmetry is broken. Hence, Coulomb drag effect assisted by momentum transfer is no longer possible and only energy transfer between the two subsystems takes place. Energy exchange between the drive and drag subsystems leads to rectification of nonequilibrium fluctuations [33] in close analogy to the ratchet effect [34, 35] with possible energy harvesting applications [36].

Reducing the dimensionality of nanoscale devices has a two-fold advantage, namely: (i) the Coulomb interaction enhances by diminishing the system size, which leads to a major dragging effect; (ii) a very small drive voltage yields a drag current generated by the excess of noise of the drive system. Both properties may play significant roles in quantum information processing. Enhanced Coulomb interaction can entangle particles in a controlled way while drag currents can be used for quantum measurement purposes, where the drag subsystem serves as the detector. In this context, drag currents can be regarded as the back-action resulting from quantum measurements in the drive system. Importantly, these systems exhibit quantum coherence. Here, we demonstrate that quantum coherence is crucial in the strongly interacting mesoscopic Coulomb drag effect.

Reference [37] proposes a simple mesoscopic setup that consists of two parallel Coulomb-coupled quantum dots attached to four separate normal electron reservoirs to generate the Coulomb drag current. Using this device, it is possible to test fundamental fluctuation relations among nonlinear transport coefficients. Both quantum dots are closely spaced so that a strong interdot Coulomb interaction is expected and the setup is thus a natural platform to observe Coulomb drag. Interdot tunneling is forbidden. The setup is analyzed employing the master equation approach, considering only sequential tunneling rates. Dot charge-state dependent tunnel barriers are key ingredients in the prediction of unidirectional drag currents, independently of the direction of the drive bias drop. A recent experiment [38] realizes the setup using a lithographically patterned AlGaAs/GaAs heterostructure and detects unidirectional drag currents as anticipated. However and in contrast to the theory of Ref. [37], the experiment shows at very low temperatures the importance of

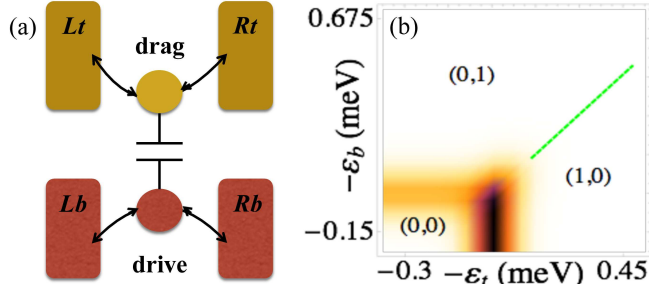


Figure 1. (a) Sketch of our device. Top dot acts as the drag subsystem held at equilibrium whereas an electrical current is driven across the bottom dot (the drive subsystem). Both dots are tunnel connected to reservoirs as indicated. Coulomb interaction between the two dots (here, represented with a capacitor) is necessary for the drag effect to happen. (b) Stability diagram as a function of the dot top level (ε_t) and the bottom dot level (ε_b). Dot occupations are denoted with (n_t, n_b) . The borders between regions with constant occupations are given by conductance values. In the limit of strong interdot interactions, there exists a unique triple point where charge fluctuates among the states $(0,0) \rightleftharpoons (0,1) \rightleftharpoons (1,0)$. The dotted line is for eye-guiding purposes.

including cotunneling processes, as demonstrated with a theoretical model that shows excellent agreement with the experimental data [38]. The role of cotunneling processes is also emphasized in Ref. [39] where a similar system is considered but with graphene reservoirs instead of normal electron reservoirs [40]. In both cases, a four-charge state model within a master equation description serves as a theoretical basis to describe the Coulomb drag effect. It is proven that nonlocal cotunneling processes contribute to the drag current to the same order as sequential tunneling events, the former being the main contribution when the dot level for the drag subsystem lies well far away from the resonant condition. In such situation, the drag current is mainly driven by high-order tunneling processes [38, 39]. Since both sequential and cotunneling events contribute to the drag effect in the formulations of Refs. [38, 39], it would be highly desirable to put forward a theoretical model that leads to cotunneling driven drag currents as opposed to the purely sequential regime discussed earlier [37].

Our aim here is then to analyze a simple model that totally suppresses drag currents induced by sequential tunneling alone. This is achieved by considering a mutual Coulomb interaction sufficiently large to discard the doubly occupied charge state. Indeed, a three-state model with solely sequential tunneling processes is unable to create drag currents. This finding emphasizes the importance of cotunneling in the physics of the drag effect. Below, we demonstrate that three states represent the minimum configuration that generates drag current around the triple point of interacting dot setups. We also show that the drag transport in this configuration must be assisted by cotunneling mechanisms unlike the four-state model employed in previous works [37, 38, 39], in which sequential contributions to the drag current are always present. The four-state model can be also employed to cancel the purely sequential drag currents but only if temperature and voltage are very low [39]. In contrast, the three-state model proposed in this work is much easier to handle and exactly nullifies the pure sequential part. Based on this simple model, we prove that the behavior and sign of the mesoscopic drag current can be controlled externally by properly engineering the energy dependence of the tunneling barriers. This can be

understood in terms of an intuitive picture of electron- and hole-type transport.

The system under consideration is plotted in Fig. 1(a). Two parallel coupled quantum dots are attached to four normal electronic reservoirs. Particle flow is indicated with arrows while electron-electron interaction occurs between the dots only (the reservoirs are assumed to be massive electrodes with good screening properties). The stability diagram for this setup is shown in Fig. 1(b). The diagram is obtained by summing the linear conductances $G_i = (dI_i/dV_i)_{V_i=0}$ ($i = t, b$) through the drag (top, t) and drive (bottom, b) dots and plotted as a function of the top (ε_t) and the bottom (ε_b) gate voltages. Here, $I_i(V_i)$ is the current (voltage) across the subsystem $i = t, b$ and (n_t, n_b) denotes the dot charge configurations, where n_t and n_b are the number of electrons on dot t and b . When the Coulomb interaction strength is very large the resulting stability diagram shown in Fig. 1(b) displays only one triple point where the doubly occupied configuration $(1, 1)$ never takes place, $(1, 0)$ and $(0, 1)$ being equally probable. We are interested in the triple point because experimental observations [38, 40] find the largest drag currents in that region of the stability diagram.

2. Theory

The model Hamiltonian

$$\mathcal{H} = \mathcal{H}_D + \mathcal{H}_C + \mathcal{H}_T \quad (1)$$

has three contributions. First,

$$\mathcal{H}_D = \sum_{i=t/b} \varepsilon_i d_i^\dagger d_i + U d_t^\dagger d_t d_b^\dagger d_b \quad (2)$$

describes the quantum dots. The operator d_i^\dagger (d_i) creates (annihilates) an electron with energy ε_i on the dot i . The interdot charging energy is denoted with U . By adjusting gate voltages appropriately, the direct tunneling between quantum dots is forbidden and can be safely neglected [38]. Second,

$$\mathcal{H}_C = \sum_{\alpha=L/R, i, k} \varepsilon_{\alpha ik} c_{\alpha ik}^\dagger c_{\alpha ik} \quad (3)$$

depicts the reservoir Hamiltonian where $c_{\alpha ik}^\dagger$ ($c_{\alpha ik}$) creates (annihilates) an electron with wavevector k and energy $\varepsilon_{\alpha ik}$ in the reservoir $\alpha i = \{Lt, Lb, Rt, Rb\}$ [Fig. 1(a)]. Finally,

$$\mathcal{H}_T = \sum_{\alpha, i, k} \left(t_{\alpha ik} c_{\alpha ik}^\dagger d_i + \text{H.c.} \right) \quad (4)$$

characterizes the coupling between the top and bottom dots and the reservoirs via the tunneling amplitudes $t_{\alpha ik}$.

We focus on the dot states, tracing out the reservoir degrees of freedom. In our system and for $U \rightarrow \infty$, there are three possible dot states $|n\rangle = \{|0\rangle, |t\rangle, |b\rangle\}$. The state $|0\rangle \equiv (0, 0)$ implies that both dots are empty, while $|t\rangle \equiv (1, 0)$ ($|b\rangle \equiv (0, 1)$) indicates that the top (bottom) dot is occupied. To lowest order in \mathcal{H}_T , the transition (sequential tunneling) rate from $|m\rangle$ to $|n\rangle$ entering or leaving the reservoir αi is given by [41]

$$\mathcal{W}_{mn}^{\alpha i} = \frac{2\pi}{\hbar} \text{Tr}_C [F_{mC} |\langle n | \mathcal{H}_T | m \rangle | m_C \rangle|^2 \delta(E_m + E_{mC} - E_n - E_{nC})], \quad (5)$$

where Tr_C designates a trace over the reservoir degrees of freedom, F_{m_C} is the thermal distribution function for the reservoir state m_C with energy E_{m_C} , and E_m and E_n are the energies of the states $|m\rangle$ and $|n\rangle$. The second-order rate in \mathcal{H}_T describes the cotunneling processes from $|m\rangle$ to $|n\rangle$ and is calculated as

$$\gamma_{mn}^{\alpha i \beta j} = \frac{2\pi}{\hbar} \text{Tr}_C [F_{m_C} |\langle n_C | \langle n | \mathcal{H}_T \mathcal{G}_0 \mathcal{H}_T | m \rangle | m_C \rangle|^2] \delta(E_m + E_{m_C} - E_n - E_{n_C}), \quad (6)$$

where \mathcal{G}_0 is the resolvent operator given by $\mathcal{G}_0 = \frac{1}{E_m - \mathcal{H}_0}$ with $\mathcal{H}_0 = \mathcal{H}_D + \mathcal{H}_C$. Conceptually, one might go further by including higher-order tunneling processes in \mathcal{H}_T but this is out of the scope of the present work. Our goal is to consider quantum coherent processes to leading order. This approximation is valid provided that the background temperature is not very low ($k_B T > \Gamma_0$, where Γ_0 is the tunnel barrier strength energy to be specified below).

Let P_n be the probability for the state $|n\rangle$. Within the master equation approach, we can write

$$\frac{d}{dt} P_0 = -(\mathcal{W}_{0t} + \mathcal{W}_{0b}) P_0 + \mathcal{W}_{t0} P_t + \mathcal{W}_{b0} P_b, \quad (7a)$$

$$\frac{d}{dt} P_t = \mathcal{W}_{0t} P_0 - (\mathcal{W}_{t0} + \gamma_{tb}) P_t + \gamma_{bt} P_b, \quad (7b)$$

$$\frac{d}{dt} P_b = \mathcal{W}_{0b} P_0 + \gamma_{tb} P_t - (\mathcal{W}_{b0} + \gamma_{bt}) P_b, \quad (7c)$$

where $\mathcal{W}_{mn} = \sum_{\alpha i} \mathcal{W}_{mn}^{\alpha i}$ and $\gamma_{mn} = \sum_{\alpha i, \beta j} \gamma_{mn}^{\alpha i \beta j}$. Importantly, the singly occupied states $|t\rangle$ and $|b\rangle$ are interconnected thanks to the cotunneling rates. In contrast, sequential tunneling processes always involve the empty state $|0\rangle$. We stress that the model described by Eq. (7) can be obtained from that of Ref. [38] first by carefully removing the doubly occupied state and only then taking the limit $U \rightarrow \infty$ in the tunneling rate expressions.

The stationary probabilities (st) can be obtained from Eq. (7) in the limit $t \rightarrow \infty$ with the aid of the probability conservation law $\sum_n P_n = 1$. The full expressions for the rates can be found in Appendix A. Let us focus on the current flowing into the left top (Lt) reservoir ($I_{\text{drag}} \equiv I_{Lt}$),

$$I_{\text{drag}} = -e [\mathcal{W}_{0t}^{Lt} P_0^{\text{st}} - (\mathcal{W}_{t0}^{Lt} + \gamma_{tb}^{LbLt} + \gamma_{tb}^{RbLt}) P_t^{\text{st}} + (\gamma_{bt}^{LtLb} + \gamma_{bt}^{LtRb}) P_b^{\text{st}}], \quad (8)$$

where e denotes the elementary positive electric charge. Crucially, when cotunneling processes are neglected the drag current identically vanishes and the doubly occupied state must be then considered. In the case of infinite charging energy treated here, the doubly occupied state is energetically forbidden and then cotunneling is required to create drag currents.

On the other hand, the drive current ($I_{\text{drive}} \equiv I_{Lb}$) is

$$\begin{aligned} \frac{I_{\text{drive}}}{-e} &= (\mathcal{W}_{0b}^{Lb} - \gamma_{00}^{RbLb} + \gamma_{00}^{LbRb}) P_0^{\text{st}} + (\gamma_{tb}^{LbLt} + \gamma_{tb}^{LbRt}) P_t^{\text{st}} \\ &\quad - (\mathcal{W}_{b0}^{Lb} + \gamma_{bb}^{RbLb} - \gamma_{bb}^{LbRb} + \gamma_{bt}^{LtLb} + \gamma_{bt}^{RtLb}) P_b^{\text{st}}. \end{aligned} \quad (9)$$

Unlike Eq. (8), Eq. (9) can be nonzero if the γ 's are nullified since a voltage is present in the drive subsystem.

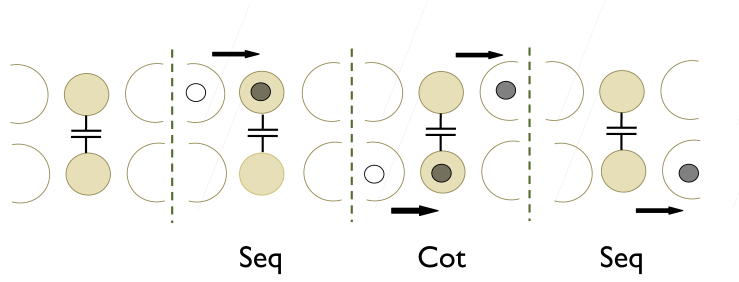


Figure 2. Characteristic transport sequence involving the drag of an electron through the top dot. Empty (filled) circles represent electrons leaving (arriving at) the different parts of the system (reservoirs or dots). Arrows indicate the transport direction. We consider a positive bias applied to the drive subsystem. Hence, we only indicate right-going processes for the lower dot. While the second and fourth panels depict sequential processes (one arrow, i.e., first order in tunneling), the third panel illustrates a cotunneling event (two arrows, i.e., second order in tunneling). The latter process is essential to drive a drag current within our model.

Calculating the stationary probabilities explicitly (see Appendix B), we find

$$I_{\text{drag}}^{(\text{seq})} \propto \Gamma_{Lt}(\varepsilon_t)\Gamma_{Rt}(\varepsilon_t) [f_{Rt}(\varepsilon_t) - f_{Lt}(\varepsilon_t)] \sum_{\alpha} \Gamma_{\alpha b}(\varepsilon_b) [1 - f_{\alpha b}(\varepsilon_b)] , \quad (10)$$

where $f_{\alpha i}(\varepsilon) = 1/[1 + e^{(\varepsilon - \mu_{\alpha i})/k_B T}]$ is the Fermi function with $\mu_{\alpha i}$ the electrochemical potential of lead αi . The dot electrochemical potentials are to be evaluated using an electrostatic model discussed in detail in Appendix C. This model is especially appealing for comparison with the experiment [38] and renders our theory gauge invariant. The hybridization widths $\Gamma_{\alpha i}(\varepsilon) = 2\pi \sum_k t_{\alpha i k}^2 \delta(\varepsilon_{\alpha i k} - \varepsilon) = 2\pi t_{\alpha i}^2(\varepsilon) \rho_{\alpha i}(\varepsilon)$ depend on the tunnel amplitude $t_{\alpha i}$ and density of states (DOS) $\rho_{\alpha i}$. Since $\mu_{Lt} = \mu_{Rt}$ in the drag system, we have $f_{Lt}(\varepsilon) = f_{Rt}(\varepsilon) \equiv f_t(\varepsilon)$ leading to a zero drag current ($I_{\text{drag}}^{(\text{seq})} = 0$) in the sequential tunneling regime within our three-state model (which corresponds physically to the case $U \rightarrow \infty$), even if the tunneling barriers are asymmetric and energy dependent. As a consequence, cotunneling events are strictly needed to generate drag currents in the configuration of three charge states.

Consider the sequence $|0\rangle \rightarrow |t\rangle \rightarrow |b\rangle \rightarrow |0\rangle$ illustrated in Fig. 2, where an electron is transported from left to right in the drag subsystem. The corresponding probability is proportional to $\mathcal{W}_{0t}^{Lt} \gamma_{tb}^{\alpha b Rt} \mathcal{W}_{b0}^{\beta b}$. The probability for the reversed process reads $\mathcal{W}_{0t}^{Rt} \gamma_{tb}^{\alpha b Lt} \mathcal{W}_{b0}^{\beta b}$. As a consequence, the net current,

$$I_{\text{drag}} \propto \sum_{\alpha, \beta} \left(\mathcal{W}_{0t}^{Lt} \gamma_{tb}^{\alpha b Rt} \mathcal{W}_{b0}^{\beta b} - \mathcal{W}_{0t}^{Rt} \gamma_{tb}^{\alpha b Lt} \mathcal{W}_{b0}^{\beta b} \right) \quad (11)$$

is clearly assisted by quantum coherent processes. We observe in Fig. 2 that two sequential transitions [i.e., $|0\rangle \rightarrow |t\rangle$ (second panel) and $|b\rangle \rightarrow |0\rangle$ (fourth panel)] are still present but they are not sufficient to drive a drag current since the middle transition ($|t\rangle \rightarrow |b\rangle$, third panel) arises solely from cotunneling.

In terms of the explicit expressions for the tunneling rates [42, 43], the drag

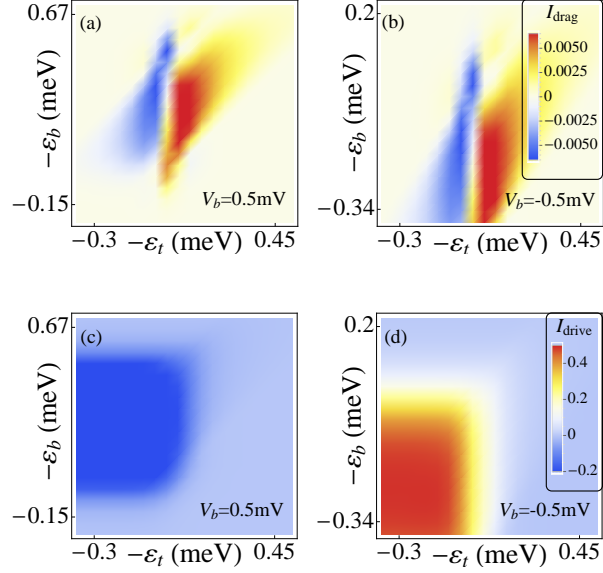


Figure 3. Drag current I_{drag} (top panels) and drive current I_{drive} (bottom panels) as a function of top (ε_t) and bottom (ε_b) dot level positions. The applied drive bias voltage is $V_b = 0.5$ mV (a,c) and $V_b = -0.5$ mV (b,d). Current is expressed in units of $e\Gamma_0/\hbar$. For reference purposes, we find a maximum value for the ratio $|I_{\text{drag}}/I_{\text{drive}}|$ of the order of 10^{-2} .

current takes the form

$$I_{\text{drag}} \propto \sum_{\alpha,\beta} \int d\varepsilon \left| \frac{1}{\varepsilon - \varepsilon_b} \right|^2 [\Gamma_{Lt}(\varepsilon_t)\Gamma_{Rt}(\varepsilon + \varepsilon_t - \varepsilon_b) - \Gamma_{Rt}(\varepsilon_t)\Gamma_{Lt}(\varepsilon + \varepsilon_t - \varepsilon_b)] \times \Gamma_{\alpha b}(\varepsilon)\Gamma_{\beta b}(\varepsilon_b)f_t(\varepsilon_t)f_{\alpha b}(\varepsilon)[1 - f_t(\varepsilon + \varepsilon_t - \varepsilon_b)][1 - f_{\beta b}(\varepsilon_b)]. \quad (12)$$

We remark that I_{drag} in Eq. (12) vanishes when $\Gamma_{\alpha i}(\varepsilon) = \Gamma_{\alpha i}$ and thus energy-dependent tunnel barriers are necessary [37, 38, 39]. We envisage that one of the tunnel barriers (top left, Lt) has a Lorentzian profile,

$$\Gamma_{Lt}(\varepsilon) = \frac{\Gamma_{Lt}}{1 + [(\varepsilon - \mu_{Lt})/D]^2}, \quad (13)$$

and the other tunnel barriers are constant, i.e., $\Gamma_{Rt}(\varepsilon) = \Gamma_{Rt}$, $\Gamma_{Lb}(\varepsilon) = \Gamma_{Lb}$, $\Gamma_{Rb}(\varepsilon) = \Gamma_{Rb}$. This model can be realized with constant tunnel amplitudes ($t_{\alpha i}(\varepsilon) = t_{\alpha i}$) while the DOS for the left top reservoir $\rho_{Lt}(\varepsilon)$ is Lorentzian and the other reservoirs have flat bands. Tailoring of the band structure in the leads can be achieved with different materials [44]. In the following we present our results for the drive and drag currents and discuss the tunability of the drag current depending on the system parameters.

3. Results

Throughout this paper, we take $\Gamma_{Lt} = \Gamma_{Rt} = (47/15)\Gamma_0$ and $\Gamma_{Lb} = \Gamma_{Rb} = \Gamma_0$ where $\Gamma_0 = 7.5 \mu\text{eV}$ is the unit of energy. These values were extracted from the

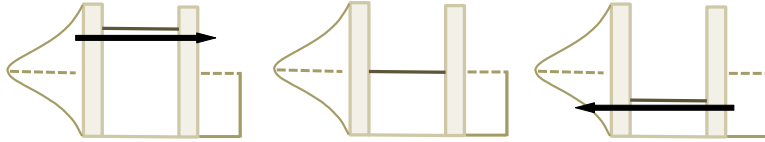


Figure 4. Sketch of the drag dot for $\mu_{Lt} = \mu_{Rt}$ (dashed lines) and three different level positions (filled dark lines). The left (right) reservoir displays a Lorentzian (flat) DOS, which determines the current direction (long arrows).

experiment [38]. The temperature is set to $k_B T = 5\Gamma_0$ and $D = 10\Gamma_0$. We evaluate the drag (I_{drag}) and drive (I_{drive}) currents as a function of ε_t and ε_b for a drive voltage $V_b \neq 0$. In Figs. 3(a) and (b), we observe that I_{drag} is strongest along the (green) dotted line shown in Fig. 1(b). Therefore, drag currents are intimately related to charge fluctuations since $I_{\text{drag}} \neq 0$ for the sequence depicted in Fig. 2, in which case the three states $|0\rangle$, $|t\rangle$, $|b\rangle$ have similar probabilities and as a consequence I_{drag} is maximal around the triple point in Fig. 1(b). Reversing the direction of V_b does not change the direction of I_{drag} but merely shifts the drag regions down following the bias window [38]. Surprisingly enough, unlike the experimental results [38] our drag current changes sign when ε_t is tuned. The phenomenon is illustrated in Fig. 4. When $\varepsilon_t > \mu_L$ (left panel) thermally excited electrons from the left reservoir can tunnel to the right lead and a negative current is then obtained (our flux sign convention states that the current is negative when it leaves the reservoir). If $\varepsilon_t < \mu_L$ (right panel) the I_{drag} direction is reversed because electrons below the Fermi energy in the right lead tend to fill the available states in the left reservoir, thus creating hole-like transport. Obviously, for $\varepsilon_t = \mu_L$ (middle panel) electron- and hole-like fluxes compensate each other and the net current is zero [see the border line between the blue and red regions in Fig. 3(a,b)]. This resembles the thermoelectric effect in quantum dots but the difference here is that here the thermal bias is zero. The common origin for both effects is the breaking of electron-hole symmetry.

The discussed effect implies that we can engineer I_{drag} by gate tuning ε_t with a suitable model for the electronic DOS at the reservoirs. This agrees with the findings of Ref. [39]. The difference is that Ref. [39] apply gate voltages to graphene reservoirs while in our double quantum dot setup we tune the energy level of the dots. Incidentally, the region in which there is an appreciable drag current is extended to ε_t values far away from resonance, as in the experiment [38]. This is due only to cotunneling processes since a purely sequential model yields sharp boundaries [37].

In Figs. 3(c) and (d) we plot the drive current as a function of the level position for a nonzero V_b . For $V_b > 0$ ($V_b < 0$) the current is negative (positive), as expected. In both cases the current is nonzero only when the ε_b is within the bias window [i.e., when $-eV_b - \varepsilon_b^0 \lesssim \varepsilon_b \lesssim \varepsilon_b^0$ where $\varepsilon_b^0 \simeq 0$ meV signals the transition $(0, 0) \rightarrow (0, 1)$ in Fig. 1(b)]. Interestingly, I_{drive} also depends on ε_t . This can be understood as follows. When the top dot level falls below the Fermi energy, the drag dot becomes occupied and transport across the drive dot remains blocked due to the strong electron-electron interaction between the dots (gating effect). Importantly, for a wide range of ε_t both currents (drag and drive) run in parallel if $V_b > 0$ [cf. Figs. 3(a) and (c)] but flow in antiparallel directions if $V_b < 0$ [cf. Figs. 3(b) and (d)]. This results in an additional degree of tunability by controlling ε_d and V_b independently.

4. Summary

We have considered a three-state model to propose a device for the observation of a drag effect that needs the presence of quantum coherent events. This is the minimal description that generate drag currents around the triple point of Coulomb coupled double quantum dots. A clever design for the attached reservoir DOS leads to a powerful tunability for the drive and drag currents. Thus, we have illustrated our findings with a model in which the left top coupling has a Lorentzian density profile and the other couplings are constant. We have demonstrated that the drag current flows in parallel or in opposite direction to the drive current by reversing the sign of the bias voltage and that the drag changes changes sign when the dot energy level is varied with an external gate potential. Our proposal hence opens a new route for the creation and manipulation of coherent drag currents in nanoscale conductors.

Acknowledgments

This work was supported by MINECO under grant No. FIS2014-52564.

Appendix A. Calculation of the transition rates

Appendix A.1. Sequential tunneling

In Eq. (5) F_{m_C} is given by

$$F_{m_C} = \frac{e^{-\beta\mathcal{H}_C}}{\text{Tr}_C [e^{-\beta\mathcal{H}_C}]}. \quad (\text{A.1})$$

As an example, we evaluate the rate $\mathcal{W}_{0i}^{\alpha i}$ from $|0\rangle$ to $|i\rangle$. Since the final state is

$$|n\rangle|n_C\rangle = d_i^\dagger c_{\alpha ik} |0\rangle|m_C\rangle, \quad (\text{A.2})$$

the rate can be written as

$$\mathcal{W}_{0i}^{\alpha i} = \frac{2\pi}{\hbar} \sum_k \sum_{m_C} F_{m_C} \left| \langle m_C | \langle 0 | c_{\alpha ik}^\dagger d_i d_i^\dagger c_{\alpha ik} | 0 \rangle | m_C \rangle \right|^2 \delta(\varepsilon_{\alpha ik} - \varepsilon_i). \quad (\text{A.3})$$

We note that

$$\sum_{m_C} F_{m_C} |\langle m_C | c_{\alpha ik}^\dagger c_{\alpha ik} | m_C \rangle|^2 = f_{\alpha i}(\varepsilon_{\alpha ik}). \quad (\text{A.4})$$

Equation (A.4) follows from the fact that $c_{\alpha ik}^\dagger c_{\alpha ik}$ can only take the values 0 or 1. Therefore, we obtain

$$\mathcal{W}_{0i}^{\alpha i} = \frac{1}{\hbar} \Gamma_{\alpha i}(\varepsilon_i) f_{\alpha i}(\varepsilon_i), \quad (\text{A.5})$$

where

$$\Gamma_{\alpha i}(\varepsilon_i) = 2\pi \sum_k t_{\alpha ik}^2 \delta(\varepsilon_{\alpha ik} - \varepsilon_i). \quad (\text{A.6})$$

The sequential tunneling rate from $|i\rangle$ to $|0\rangle$ can be similarly found,

$$\mathcal{W}_{i0}^{\alpha i} = \frac{1}{\hbar} \Gamma_{\alpha i}(\varepsilon_i) [1 - f_{\alpha i}(\varepsilon_i)]. \quad (\text{A.7})$$

Appendix A.2. Cotunneling

The cotunneling rate from $|m\rangle$ to $|n\rangle$ is given by Eq. (6). For energy dependent tunnel broadenings, we find

$$\gamma_{00}^{\alpha i \beta i} = \frac{1}{2\pi\hbar} \int d\varepsilon \left| \frac{1}{\varepsilon - \varepsilon_i + i\eta} \right|^2 \Gamma_{\alpha i}(\varepsilon) \Gamma_{\beta i}(\varepsilon) f_{\alpha i}(\varepsilon) [1 - f_{\beta i}(\varepsilon)], \quad (\text{A.8a})$$

$$\gamma_{ii}^{\alpha i \beta i} = \frac{1}{2\pi\hbar} \int d\varepsilon \left| \frac{1}{\varepsilon - \varepsilon_i + i\eta} \right|^2 \Gamma_{\alpha i}(\varepsilon) \Gamma_{\beta i}(\varepsilon) f_{\alpha i}(\varepsilon) [1 - f_{\beta i}(\varepsilon)], \quad (\text{A.8b})$$

$$\gamma_{i\bar{i}}^{\alpha \bar{i} \beta i} = \frac{1}{2\pi\hbar} \int d\varepsilon \left| \frac{1}{\varepsilon - \varepsilon_{\bar{i}} + i\eta} \right|^2 \Gamma_{\alpha \bar{i}}(\varepsilon) \Gamma_{\beta i}(\varepsilon + \varepsilon_i - \varepsilon_{\bar{i}}) f_{\alpha \bar{i}}(\varepsilon) [1 - f_{\beta i}(\varepsilon + \varepsilon_i - \varepsilon_{\bar{i}})], \quad (\text{A.8c})$$

where $\bar{i} = b/t$ for $i = t/b$. Since the intermediate virtual states acquire a finite lifetime during the tunneling processes, we added a small positive parameter η . We note that in contrast to Ref. [38] we here explicitly write down the expression for $\gamma_{00}^{\alpha i \beta i}$ since it enters the expression for I_{drive} . In Ref. [38] the calculation of this rate is not needed because only I_{drag} is shown.

We now use the identity

$$f_a(\varepsilon_i) [1 - f_b(\varepsilon_j)] = \frac{1}{2} n_B(\varepsilon_i - \varepsilon_j - \mu_a + \mu_b) [\tanh(\beta(\varepsilon_i - \mu_a)/2) - \tanh(\beta(\varepsilon_j - \mu_b)/2)], \quad (\text{A.9})$$

where $n_B(x) = 1/(\exp(\beta x) + 1)$. Here, $\tanh(z)$ can be expressed as

$$\tanh(z) = -\frac{i}{\pi} \left[\Psi\left(\frac{1}{2} + i\frac{z}{\pi}\right) - \Psi\left(\frac{1}{2} - i\frac{z}{\pi}\right) \right], \quad (\text{A.10})$$

where $\Psi(z)$ denotes the digamma function. Employing the fact that $\Psi(\frac{1}{2} + i\frac{z}{2\pi})$ has the poles in the upper halfplane at the locations $z = i\pi(1/2 + n)$, where $n \in \mathbb{N}$, while the poles of $\Psi(\frac{1}{2} - i\frac{z}{2\pi})$ are in the lower halfplane at the locations $z = -i\pi(1/2 + n)$, the integrals in Eqs. (A.8) can then be easily calculated. In the final stage, we expand the results in powers of η . Those terms scaling as $1/\eta$ are removed since they are indeed sequential tunneling processes and cannot be counted twice. Then, we take the limit $\eta \rightarrow 0$ and find

$$\gamma_{00/bb}^{\alpha b \beta b} = \frac{\beta}{4\pi^2\hbar} \Gamma_{\alpha b} \Gamma_{\beta b} n_B(\mu_{\beta b} - \mu_{\alpha b}) \Im \left[\Psi^{(1)}\left(\frac{1}{2} + i\beta \frac{\varepsilon_b - \mu_{\alpha b}}{2\pi}\right) - \Psi^{(1)}\left(\frac{1}{2} + i\beta \frac{\varepsilon_b - \mu_{\beta b}}{2\pi}\right) \right], \quad (\text{A.11a})$$

$$\begin{aligned} \gamma_{t\bar{t}}^{\alpha b L t} &= \frac{\Gamma_{\alpha b} \Gamma_{L t}}{2\pi\hbar} n_B(\varepsilon_b - \varepsilon_t + \mu_{L t} - \mu_{\alpha b}) \\ &\times \left\{ \frac{D^2}{D^2 + (\varepsilon_t - \mu_{L t})^2} \Im \left[\frac{2i(\varepsilon_t - \mu_{L t})}{D^2 + (\varepsilon_t - \mu_{L t})^2} \left(\Psi\left(\frac{1}{2} + i\beta \frac{\varepsilon_b - \mu_{\alpha b}}{2\pi}\right) - \Psi\left(\frac{1}{2} + i\beta \frac{\varepsilon_t - \mu_{L t}}{2\pi}\right) \right) \right. \right. \\ &\quad \left. \left. + \frac{\beta}{2\pi} \left(\Psi^{(1)}\left(\frac{1}{2} + i\beta \frac{\varepsilon_b - \mu_{\alpha b}}{2\pi}\right) - \Psi^{(1)}\left(\frac{1}{2} + i\beta \frac{\varepsilon_t - \mu_{L t}}{2\pi}\right) \right) \right] \right. \\ &\left. + \frac{1}{D} \Im \left[\frac{D^2}{(\varepsilon_u - \mu_{L t} + iD)^2} \left(\Psi\left(\frac{1}{2} + \frac{\beta D}{2\pi} + i\beta \frac{\varepsilon_b - \varepsilon_t - \mu_{\alpha b} + \mu_{L t}}{2\pi}\right) - \Psi\left(\frac{1}{2} + \frac{\beta D}{2\pi}\right) \right) \right] \right\}, \quad (\text{A.11b}) \end{aligned}$$

$$\begin{aligned}
\gamma_{bt}^{Lt\alpha b} &= \frac{\Gamma_{Lt}\Gamma_{\alpha b}}{2\pi\hbar} n_B(\varepsilon_t - \varepsilon_b + \mu_{\alpha b} - \mu_{Lt}) \\
&\times \left\{ \frac{D^2}{D^2 + (\varepsilon_t - \mu_{Lt})^2} \Im \left[\frac{2i(\varepsilon_t - \mu_{Lt})}{D^2 + (\varepsilon_t - \mu_{Lt})^2} \left(\Psi \left(\frac{1}{2} + i\beta \frac{\varepsilon_t - \mu_{Lt}}{2\pi} \right) - \Psi \left(\frac{1}{2} + i\beta \frac{\varepsilon_b - \mu_{\alpha b}}{2\pi} \right) \right) \right. \right. \\
&\quad \left. \left. + \frac{\beta}{2\pi} \left(\Psi^{(1)} \left(\frac{1}{2} + i\beta \frac{\varepsilon_t - \mu_{Lt}}{2\pi} \right) - \Psi^{(1)} \left(\frac{1}{2} + i\beta \frac{\varepsilon_b - \mu_{\alpha b}}{2\pi} \right) \right) \right] \right. \\
&\left. + \frac{1}{D} \Im \left[\frac{D^2}{(\varepsilon_u - \mu_{Lt} + iD)^2} \left(\Psi \left(\frac{1}{2} + \frac{\beta D}{2\pi} \right) - \Psi \left(\frac{1}{2} + \frac{\beta D}{2\pi} + i\beta \frac{\varepsilon_b - \varepsilon_t - \mu_{\alpha b} + \mu_{Lt}}{2\pi} \right) \right) \right] \right\}, \tag{A.11c}
\end{aligned}$$

$$\gamma_{tb}^{\alpha b Rt} = \frac{\beta \Gamma_{\alpha b} \Gamma_{Rt}}{4\pi^2 \hbar} n_B(\varepsilon_b - \varepsilon_t + \mu_{Rt} - \mu_{\alpha b}) \Im \left[\Psi^{(1)} \left(\frac{1}{2} + i\beta \frac{\varepsilon_b - \mu_{\alpha b}}{2\pi} \right) - \Psi^{(1)} \left(\frac{1}{2} + i\beta \frac{\varepsilon_t - \mu_{Rt}}{2\pi} \right) \right], \tag{A.11d}$$

$$\gamma_{bt}^{Rt\alpha b} = \frac{\beta \Gamma_{Rt} \Gamma_{\alpha b}}{4\pi^2 \hbar} n_B(\varepsilon_t - \varepsilon_b + \mu_{\alpha b} - \mu_{Rt}) \Im \left[\Psi^{(1)} \left(\frac{1}{2} + i\beta \frac{\varepsilon_t - \mu_{Rt}}{2\pi} \right) - \Psi^{(1)} \left(\frac{1}{2} + i\beta \frac{\varepsilon_b - \mu_{\alpha b}}{2\pi} \right) \right]. \tag{A.11e}$$

Unlike Ref. [38], we here obtain the expression for the rate $\gamma_{00/bb}^{\alpha b \beta b}$ in order to compute I_{drag} .

Appendix B. Drag and Drive Currents in the Sequential Tunneling Limit

In the stationary limit, Eqs. (7) in combination with the probability conservation law yield

$$P_0^{\text{st}} = \frac{\mathcal{W}_{t0}\mathcal{W}_{b0} + \gamma_{bt}\mathcal{W}_{t0} + \gamma_{tb}\mathcal{W}_{b0}}{\mathcal{D}}, \tag{B.1a}$$

$$P_t^{\text{st}} = \frac{\mathcal{W}_{b0}\mathcal{W}_{0t} + \mathcal{W}_{0b}\gamma_{bt} + \gamma_{bt}\mathcal{W}_{0t}}{\mathcal{D}}, \tag{B.1b}$$

$$P_b^{\text{st}} = \frac{\mathcal{W}_{t0}\mathcal{W}_{0b} + \mathcal{W}_{0t}\gamma_{tb} + \gamma_{tb}\mathcal{W}_{0b}}{\mathcal{D}}, \tag{B.1c}$$

where $\mathcal{D} = (\mathcal{W}_{0b} + \mathcal{W}_{0t})(\gamma_{bt} + \gamma_{tb}) + (\gamma_{bt} + \mathcal{W}_{0b})\mathcal{W}_{t0} + (\mathcal{W}_{0t} + \mathcal{W}_{t0} + \gamma_{tb})\mathcal{W}_{b0}$. In Eqs. (B.1), $\mathcal{W}_{t0} = \sum_{\alpha} \mathcal{W}_{t0}^{\alpha t}$, $\mathcal{W}_{b0} = \sum_{\alpha} \mathcal{W}_{b0}^{\alpha b}$, $\mathcal{W}_{0t} = \sum_{\alpha} \mathcal{W}_{0t}^{\alpha t}$, and $\mathcal{W}_{0b} = \sum_{\alpha} \mathcal{W}_{0b}^{\alpha b}$ are the total sequential rates whilst $\gamma_{tb} = \sum_{\alpha, \beta} \gamma_{tb}^{\alpha \beta t}$ and $\gamma_{bt} = \sum_{\alpha, \beta} \gamma_{bt}^{\alpha \beta b}$ denote the total cotunneling rates.

To emphasize the role of the cotunneling processes in our three-state model, we now consider only the sequential rates. The stationary probabilities then reduce to

$$P_0^{\text{seq, st}} = \frac{\mathcal{W}_{t0}\mathcal{W}_{b0}}{\mathcal{W}_{0b}\mathcal{W}_{t0} + \mathcal{W}_{0t}\mathcal{W}_{b0} + \mathcal{W}_{t0}\mathcal{W}_{b0}}, \tag{B.2a}$$

$$P_t^{\text{seq, st}} = \frac{\mathcal{W}_{b0}\mathcal{W}_{0t}}{\mathcal{W}_{0b}\mathcal{W}_{t0} + \mathcal{W}_{0t}\mathcal{W}_{b0} + \mathcal{W}_{t0}\mathcal{W}_{b0}}, \tag{B.2b}$$

$$P_b^{\text{seq, st}} = \frac{\mathcal{W}_{t0}\mathcal{W}_{0b}}{\mathcal{W}_{0b}\mathcal{W}_{t0} + \mathcal{W}_{0t}\mathcal{W}_{b0} + \mathcal{W}_{t0}\mathcal{W}_{b0}}. \tag{B.2c}$$

The drag current due to the sequential tunneling [see Eq. (8) in the absence of the cotunneling processes] becomes

$$\begin{aligned}
I_{\text{drag}} &= -e (\mathcal{W}_{0t}^{Lt} P_0^{\text{seq, st}} - \mathcal{W}_{t0}^{Lt} P_t^{\text{seq, st}}) \\
&= -e \frac{(\mathcal{W}_{t0}^{Rt} \mathcal{W}_{0t}^{Lt} - \mathcal{W}_{t0}^{Lt} \mathcal{W}_{0t}^{Rt}) \mathcal{W}_{b0}}{\mathcal{W}_{0b}\mathcal{W}_{t0} + \mathcal{W}_{0t}\mathcal{W}_{b0} + \mathcal{W}_{t0}\mathcal{W}_{b0}}. \tag{B.3}
\end{aligned}$$

Using Eqs. (A.5) and (A.7), we find Eq. (10). Following the same reasoning, it can be shown that the drive current becomes

$$I_{\text{drive}} \propto \Gamma_{Lb}(\varepsilon_b)\Gamma_{Rb}(\varepsilon_b) \times \{[1 - f_{Rb}(\varepsilon_b)]f_{Lb}(\varepsilon_b) - [1 - f_{Lb}(\varepsilon_b)]f_{Rb}(\varepsilon_b)\}. \quad (\text{B.4})$$

In this case, the left and right bottom reservoirs have different chemical potentials [i.e., $f_{Lb}(\varepsilon_b) \neq f_{Rb}(\varepsilon_b)$], thereby the drive current does not vanish unlike the sequential drag current. We conclude that the cotunneling processes are the essential ingredient to get a drag current in the minimal three-state model. This is in contrast to the four-state model in which even the sequential tunneling processes alone can induce a drag current [37].

Appendix C. Electrostatic Model

With the geometry shown in Fig. C1, the electrostatic equations for the charges Q_t and Q_b are given by

$$Q_t = \sum_{\alpha=1}^4 C_{\alpha t}(\phi_t - V_{\alpha}) + C(\phi_t - \phi_b), \quad (\text{C.1a})$$

$$Q_b = \sum_{\alpha=1}^4 C_{\alpha b}(\phi_b - V_{\alpha}) + C(\phi_b - \phi_t). \quad (\text{C.1b})$$

To shorten the notation, we set $V_1 = V_{Lt}$, $V_2 = V_{Rt}$, $V_3 = V_{Lb}$ and $V_4 = V_{Rb}$. Solving Eqs. (C.1), we find the internal potentials ϕ_t and ϕ_b

$$\phi_t = \frac{1}{K} \left[\sum_{\alpha} C_{\alpha b}(Q_t + \sum_{\beta} C_{\beta t}V_{\beta}) + C(Q_t + Q_b + \sum_{\alpha} \sum_{i=t/b} C_{\alpha i}V_{\alpha}) \right], \quad (\text{C.2a})$$

$$\phi_b = \frac{1}{K} \left[\sum_{\alpha} C_{\alpha t}(Q_b + \sum_{\beta} C_{\beta b}V_{\beta}) + C(Q_t + Q_b + \sum_{\alpha} \sum_{i=t/b} C_{\alpha i}V_{\alpha}) \right], \quad (\text{C.2b})$$

where

$$K = \sum_{\alpha} C_{\alpha t} \sum_{\beta} C_{\beta b} + C \sum_{\alpha} \sum_{i=t/b} C_{\alpha i}. \quad (\text{C.3})$$

The potential energies with N_t and N_b excess electrons then take the form

$$U_t(N_t, N_b) = \int_0^{eN_t} dQ_t \phi_t(Q_t, Q_b), \quad (\text{C.4a})$$

$$U_b(N_t, N_b) = \int_0^{eN_b} dQ_b \phi_b(Q_t, Q_b), \quad (\text{C.4b})$$

which become

$$U_t(N_t, N_b) = \frac{eN_t}{2K} \left[\sum_{\alpha} C_{\alpha b}(eN_t + 2 \sum_{\beta} C_{\beta t}V_{\beta}) + C(eN_t + 2eN_b + 2 \sum_{\alpha} \sum_{i=t/b} C_{\alpha i}V_{\alpha}) \right], \quad (\text{C.5a})$$

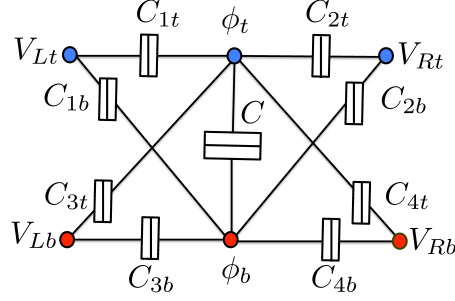


Figure C1. Electrostatic model for the double quantum dot system.

$$U_b(N_t, N_b) = \frac{eN_b}{2K} \left[\sum_{\alpha} C_{\alpha t} (eN_b + 2 \sum_{\beta} C_{\beta b} V_{\beta}) + C(2eN_t + eN_b + 2 \sum_{\alpha} \sum_{i=t/b} C_{\alpha i} V_{\alpha}) \right]. \quad (\text{C.5b})$$

In the uncharged case, the electrochemical potential (effective level) of top or bottom dot can be written as

$$\varepsilon_{t0}^{\text{eff}} = E_t - E_0 = \varepsilon_t + U_t(1, 0) - U_t(0, 0), \quad (\text{C.6a})$$

$$\varepsilon_{b0}^{\text{eff}} = E_b - E_0 = \varepsilon_b + U_b(0, 1) - U_b(0, 0), \quad (\text{C.6b})$$

where E_i is the single-particle kinetic energy plus the internal potential energy. Equation (C.6) is the energy required to add one electron into top or bottom dot when both levels are empty:

$$\varepsilon_{t0}^{\text{eff}} = \varepsilon_t + \frac{e}{2K} \left[\sum_{\alpha} C_{\alpha b} (e + 2 \sum_{\beta} C_{\beta t} V_{\beta}) + C(e + 2 \sum_{\alpha} \sum_{i=t/b} C_{\alpha i} V_{\alpha}) \right], \quad (\text{C.7a})$$

$$\varepsilon_{b0}^{\text{eff}} = \varepsilon_b + \frac{e}{2K} \left[\sum_{\alpha} C_{\alpha t} (e + 2 \sum_{\beta} C_{\beta b} V_{\beta}) + C(e + 2 \sum_{\alpha} \sum_{i=t/b} C_{\alpha i} V_{\alpha}) \right]. \quad (\text{C.7b})$$

The Fermi functions are evaluated at $\varepsilon_{i0}^{\text{eff}} - \mu_{\alpha}$, where $\mu_{\alpha} = E_F + eV_{\alpha}$ with E_F the

common Fermi energy:

$$\varepsilon_{t0}^{\text{eff}} - \mu_1 = \varepsilon_t - E_F + \frac{1}{K} \left[\frac{e^2 (\sum_{\alpha} C_{\alpha b} + C)}{2} + e \sum_{\alpha, \beta} C_{\alpha b} C_{\beta t} V_{\beta 1} + e \sum_{\alpha, i} C C_{\alpha i} V_{\alpha 1} \right], \quad (\text{C.8a})$$

$$\varepsilon_{t0}^{\text{eff}} - \mu_2 = \varepsilon_t - E_F + \frac{1}{K} \left[\frac{e^2 (\sum_{\alpha} C_{\alpha b} + C)}{2} + e \sum_{\alpha, \beta} C_{\alpha b} C_{\beta t} V_{\beta 2} + e \sum_{\alpha, i} C C_{\alpha i} V_{\alpha 2} \right], \quad (\text{C.8b})$$

$$\varepsilon_{b0}^{\text{eff}} - \mu_3 = \varepsilon_b - E_F + \frac{1}{K} \left[\frac{e^2 (\sum_{\alpha} C_{\alpha t} + C)}{2} + e \sum_{\alpha, \beta} C_{\alpha t} C_{\beta b} V_{\beta 3} + e \sum_{\alpha, i} C C_{\alpha i} V_{\alpha 3} \right], \quad (\text{C.8c})$$

$$\varepsilon_{b0}^{\text{eff}} - \mu_4 = \varepsilon_b - E_F + \frac{1}{K} \left[\frac{e^2 (\sum_{\alpha} C_{\alpha t} + C)}{2} + e \sum_{\alpha, \beta} C_{\alpha t} C_{\beta b} V_{\beta 4} + e \sum_{\alpha, i} C C_{\alpha i} V_{\alpha 4} \right], \quad (\text{C.8d})$$

Here, $V_{\alpha\beta} = V_{\alpha} - V_{\beta}$ and our model is gauge invariant as should be.

For $U \rightarrow \infty$, the doubly occupied state is forbidden, which amounts to taking the limit $C \rightarrow \infty$. We then have

$$\varepsilon_{t0}^{\text{eff}} - \mu_1 = \varepsilon_t - E_F + \frac{e^2}{2C_{\Sigma}} + \frac{e}{C_{\Sigma}} \sum_{\alpha, i} C_{\alpha i} V_{\alpha 1}, \quad (\text{C.9a})$$

$$\varepsilon_{t0}^{\text{eff}} - \mu_2 = \varepsilon_t - E_F + \frac{e^2}{2C_{\Sigma}} + \frac{e}{C_{\Sigma}} \sum_{\alpha, i} C_{\alpha i} V_{\alpha 2}, \quad (\text{C.9b})$$

$$\varepsilon_{b0}^{\text{eff}} - \mu_3 = \varepsilon_b - E_F + \frac{e^2}{2C_{\Sigma}} + \frac{e}{C_{\Sigma}} \sum_{\alpha, i} C_{\alpha i} V_{\alpha 3}, \quad (\text{C.9c})$$

$$\varepsilon_{b0}^{\text{eff}} - \mu_4 = \varepsilon_b - E_F + \frac{e^2}{2C_{\Sigma}} + \frac{e}{C_{\Sigma}} \sum_{\alpha, i} C_{\alpha i} V_{\alpha 4} \quad (\text{C.9d})$$

with

$$C_{\Sigma} = \sum_{\alpha, i} C_{\alpha i}. \quad (\text{C.10})$$

For the numerical simulations of Sec. 3 we use in units of e^2/Γ_0 the values $C_{1t} = 1/202$, $C_{2t} = 1/815$, $C_{3b} = 1/1485$, $C_{4b} = 1/177$ and $C_{1b} = C_{2b} = C_{3t} = C_{4t} = 0$. These values have been extracted from the experimental stability diagrams of Ref. [38], as reported in its Supplementary Material [45].

References

- [1] Rojo A G 1999 *J. Phys.: Condens. Matter* **11** R31
- [2] Narozhny B N and Levchenko A 2016 *Rev. Mod. Phys.* **88** 025003
- [3] Pogrebinskii M B 1977 *Fiz. Tekh. Poluprovodn.* **11** 637 [*Sov. Phys.-Semicond.* **11** 372]
- [4] Price P J 1983 *Physica B* **117-118** 750
- [5] Solomon P M, Price P J, Frank D J and La Tulipe D C 1989 *Phys. Rev. Lett.* **63** 2508

- [6] Gramila T J, Eisenstein J P, MacDonald A H, Pfeiffer L N and West K W 1991 *Phys. Rev. Lett.* **66** 1216; 1993 *Phys. Rev. B* **47** 12957; 1994 *Physica B* **197** 442
- [7] Sivan U, Solomon P M and Shtrikman H 1992 *Phys. Rev. Lett.* **68** 1196
- [8] Hill N P R, Nicholls J T, Linfield E H, Pepper M, Ritchie D A, Hamilton A R and Jones G A C 1996 *J. Phys.: Condens. Matter* **8** L557
- [9] Rubel H, Fischer A, Dietsche W, von Klitzing K and Eberl K 1997 *Phys. Rev. Lett.* **78** 1763
- [10] Lilly M P, Eisenstein J P, Pfeiffer L N and West K W 1998 *Phys. Rev. Lett.* **80** 1714
- [11] Feng X G, Zelakiewicz S, Noh H, Ragucci T J and Gramila T J, Pfeiffer L N and West K W 1998 *Phys. Rev. Lett.* **81** 3219
- [12] Lok J G S, Kraus S, Pohlt M, Dietsche W, von Klitzing K, Wegscheider W and Bichler M 2001 *Phys. Rev. B* **63** 041305(R)
- [13] Kellogg M, Spielman I B, Eisenstein J P, Pfeiffer L N and West K W 2002 *Phys. Rev. Lett.* **88** 126804
- [14] Kellogg M, Eisenstein J P, Pfeiffer L N and West K W 2003 *Phys. Rev. Lett.* **90** 246801
- [15] Muraki K, J. G. S. Lok, S. Kraus, W. Dietsche, K. von Klitzing, D. Schuh, M. Bichler, and W. Wegscheider 2004 *Phys. Rev. Lett.* **92** 246801
- [16] Tutuc E, Pillarisetty R and Shayegan M 2009 *Phys. Rev. B* **79** 041303(R)
- [17] Nandi D, Finck A D K, Eisenstein J P, Pfeiffer L N and West K W 2012 *Nature* **488** 481
- [18] Debray P, Vasilopoulos P, Raichev O, Perrin R, Rahman M and Mitchel W C 2000 *Physica E* **6** 694
- [19] Debray P, Zverev V, Raichev O, Klesse R, Vasilopoulos P and Newrock R S 2001 *J. Phys.: Condens. Matter* **13** 3389
- [20] Yamamoto M, Stopa M, Tokura Y, Hirayama Y, Tarucha S 2002 *Physica E* **12** 726; 2006 *Science* **313** 204
- [21] Laroche D, Gervais G, Lilly M P and Reno J L 2011 *Nature Nanotechnol.* **6** 793; 2014 *Science* **343** 631
- [22] Kim S, Jo I, Nah J, Yao Z, Banerjee S K and Tutuc E 2011 *Phys. Rev. B* **83** 161401(R)
- [23] Gorbachev R V, Geim A K, Katsnelson M I, Novoselov K S, Tudorovskiy T, Grigorieva I V, MacDonald A H, Morozov S V, Watanabe K, Taniguchi T and Ponomarenko L A 2012 *Nature Phys.* **8** 896
- [24] Kim S and Tutuc E 2012 *Solid State Commun.* **152** 1283
- [25] Chen H and Appenzeller J 2013 *Nano Res.* **6** 897
- [26] Gamucci A, Spirito D, Carrega M, Karmakar B, Lombardo A, Bruna M, Pfeiffer L N, West K W, Ferrari A C, Polini M and Pellegrini V 2014 *Nature Commun.* **5** 5824
- [27] Lee K, Xue J, Dillen D C, Watanabe K, Taniguchi T and Tutuc E 2016 *Phys. Rev. Lett.* **117** 046803
- [28] Averin D V, Korotkov A N, Nazarov Yu V 1991 *Phys. Rev. Lett.* **66** 2818
- [29] Matters M, Versluis J J and Mooij J E 1997 *Phys. Rev. Lett.* **78** 2469
- [30] Shimizu M, Yamamoto M, Stopa M, Honda M and Tarucha S 2005 *Physica E* **26** 460
- [31] Shinkai G, Hayashi T, Ota T, Muraki K and Fujisawa T 2009 *Appl. Phys. Express* **2** 081101
- [32] Khrapai V S, Ludwig S, Kotthaus J P, Tranitz H P and Wegscheider W 2007 *Phys. Rev. Lett.* **99** 096803
- [33] Levchenko A and Kamenev A 2008 *Phys. Rev. Lett.* **101** 216806
- [34] Astumian R D 2008, *Phys. Rev. Lett.* **101** 046802
- [35] Moldoveanu V and Tanatar B 2010 *Phys. Rev. B* **82** 205312
- [36] Hussein R and Kohler S 2015 *Annalen der Physik* **527** 610
- [37] Sánchez R, López R, Sánchez D and Büttiker M 2010 *Phys. Rev. Lett.* **104** 076801
- [38] Keller A J, Lim J S, Sánchez D, López R, Amasha S, Katine J A, Shtrikman H and Goldhaber-Gordon D 2016 *Phys. Rev. Lett.* **117** 066602
- [39] Kaasbjerg K and Jauho A-P 2016 *Phys. Rev. Lett.* **116** 196801
- [40] Bischoff D, Eich M, Zilberberg O, Rössler C, Ihn T and Ensslin K 2015 *Nano Lett.* **15** 6003
- [41] Bruus H and Flensberg K 2004 *Many-Body Quantum Theory in Condensed Matter Physics* (Oxford University Press).
- [42] Averin D 1994 *Physica B* **194-196** 979
- [43] Turek M and Matveev K A 2002 *Phys. Rev. B* **65** 115332
- [44] *Handbook of the Band Structure of Elemental Solids*, edited by D. A. Papaconstantopoulos (Plenum, New York, 1986).
- [45] See Table I in <https://journals.aps.org/prl/supplemental/10.1103/PhysRevLett.117.066602/supp.pdf>